



WNK1 Alleviates Chloride Efflux-Induced NLRP3 Inflammasome Activation and Subsequent Neuroinflammation in Early Brain Injury Following Subarachnoid Hemorrhage

Panpan Zhao¹ · Huimiao Feng² · Xinyu Zhou³ · Jingyuan Zhou¹ · Fangbo Hu¹ · Taotao Hu¹ · Yong Sun¹ 

Received: 3 September 2024 / Accepted: 3 March 2025

© Center for Excellence in Brain Science and Intelligence Technology, Chinese Academy of Sciences 2025

Abstract The nod-like receptor family pyrin domain containing 3 (NLRP3) inflammasome plays a crucial role in the prognosis of subarachnoid hemorrhage (SAH). WNK1 kinase negatively regulates NLRP3 in various inflammatory conditions, but its role in early brain injury (EBI) after SAH remains unclear. In this study, we used an *in vivo* SAH model in rats/mice and AAV-WNK1 intraventricular injection to investigate its neuroprotective mechanisms. WNK1 expression was significantly reduced in SAH patient blood and SAH model brain tissue, correlating negatively with microglial activation. AAV-WNK1 alleviated brain edema, neuronal necrosis, behavioral deficits, and inflammation by inhibiting NLRP3 inflammasome activation.

In hemin-stimulated BV-2 cells, WNK1 overexpression reduced NLRP3 activation and inflammatory cytokines. Chloride counteracted WNK1's inhibitory effects, and WNK1 suppressed P2X7R-induced NLRP3 activation. Mechanistically, WNK1 functioned *via* the OXSR1/STK39 pathway. These findings highlight WNK1 as a key regulator of intracellular chloride balance and neuroinflammation, presenting a potential therapeutic target for SAH treatment.

Keywords WNK1 · Subarachnoid hemorrhage · Chloride · NLRP3 inflammasome · Neuroinflammation · P2X7R

Panpan Zhao and Huimiao Feng contributed equally to this work.

Supplementary Information The online version contains supplementary material available at <https://doi.org/10.1007/s12264-025-01414-3>.

✉ Yong Sun
sunyong@njmu.edu.cn

¹ Neurosurgery Department, Institute of Neuroscience, Lianyungang Clinical College of Nanjing Medical University, The Affiliated Lianyungang Hospital of Xuzhou Medical University, The First People's Hospital of Lianyungang, 222000, China

² Jiangsu Key Laboratory of Marine Pharmaceutical Compound Screening, College of Pharmacy, Jiangsu Ocean University, Lianyungang 222005, China

³ Department of Neurology, Institute of Neuroscience, Lianyungang Clinical College of Nanjing Medical University, The First Affiliated Hospital of Kangda College of Nanjing Medical University, The Affiliated Lianyungang Hospital of Xuzhou Medical University, The First People's Hospital of Lianyungang, Lianyungang 222000, China

Introduction

Subarachnoid hemorrhage (SAH), which is caused primarily by the rupture of intracranial aneurysms, has high mortality and morbidity rates, affects younger populations, and results in significant societal losses [1]. Epidemiological studies indicate that one-third of SAH patients die within 24–72 h [2, 3]. Early brain injury (EBI) is the primary cause of death and delayed neurological damage following SAH [2, 4]. One crucial pathological process of EBI is neuroinflammation-induced post-SAH [5, 6], which can lead to life-threatening complications, such as vasospasm, chronic hydrocephalus, epileptic seizures, delayed cerebral ischemia, and systemic or localized infections. Thus, targeting neuroinflammation could alleviate EBI and effectively improve neurological outcomes post-SAH.

Microglia, key innate immune cells, play a vital role after SAH [7] and can be activated by neurotoxic factors [8]. Numerous studies have reported that during SAH, activated microglia initially develop into the classical M1 phenotype before transitioning to the M2 phenotype [9, 10]. The

NLRP3 (NLR family pyrin domain containing 3) inflammasome regulates microglial activation to modulate inflammatory responses [11]. SAH activates nuclear factor kappa B (NF- κ B), promoting the translocation of the p65 subunit into the nucleus and increasing the protein levels of downstream proinflammatory cytokines (IL-1 β , IL-6, TNF- α) and NLRP3. These effects collectively exacerbate the neurological deficits post-SAH [12]. Inhibiting the NLRP3 inflammasome can relieve neurological deficits and improve post-SAH neurobehavioural outcomes [13]. Therefore, understanding the activation mechanisms of the NLRP3 inflammasome in SAH is crucial for its prevention and treatment.

Adenosine triphosphate (ATP), a typical damaging molecule, is released from damaged neurons after injury and rapidly attracts microglia to the damaged area, thus promoting an inflammatory response that may exacerbate secondary brain injury after SAH [14]. P2X7R, an ATP-dependent gated ion channel, is sensitive to changes in the extracellular ATP concentration, with high extracellular ATP levels inducing the opening of the channel, leading to intracellular K⁺ efflux [15]. This change in intracellular and extracellular K⁺ concentrations induces NEK7 binding with NLRP3, thus promoting NLRP3 oligomerization. These effects induce the assembly of NLRP3-ASC-procaspase-1, inflammasome activation, caspase-1 activation, and increased release of the proinflammatory cytokine IL-1 β [16–18]. Studies have shown that WNK1 senses a reduction in intracellular Cl[−] and undergoes autophosphorylation. WNK1 phosphorylation mediates the phosphorylation of its downstream targets STK39/OXSR1 [19, 20], which then activate the cation-Cl[−] cotransporter to restore the ion concentration and inhibit further Cl[−] efflux [21, 22]. The restoration of normal intracellular Cl[−] concentration further inhibits NLRP3 inflammasome activation [23].

This study aimed to explore how WNK1 regulates NLRP3 inflammasome activation after SAH. Results showed that SAH induces low expression of WNK1, and WNK1 inhibits neurological deficits and neuroinflammation in EBI after SAH. Mechanistically, WNK1 inhibits P2X7R-induced NLRP3 inflammasome activation by sensing the reduction of intracellular chloride ions and activating the OXSR1/STK39 pathway. The identified targets will improve the prognosis of SAH patients.

Materials and Methods

Ethical Approval

All animal experiments in this study have been approved by the Jiangsu Ocean Animal Ethics Committee (No. JOUH23010) with the National Institutes of Health (NIH) Guide for the Care and Use of Laboratory Animals. All

patients' blood assays were approved by the Lianyungang First People's Hospital Medical Ethics Committee (Approval No.: KY-20231106003-02).

SAH Patients and Blood Samples

This study was approved by the Medical Ethics Committee of Lianyungang First People's Hospital (Approval No. KY-20231106003-02), and informed consent was given by all participants or their legal representatives. The study included 16 patients admitted to Lianyungang First People's Hospital within 3 days of SAH onset from May 2023 to May 2024.

The inclusion criteria for SAH patients were as follows: (1) SAH confirmed by head CT; (2) anterior circulation single aneurysm rupture verified by brain CTA and digital subtraction angiography; (3) time from onset to hospital admission \leq 8 h; (4) age between 18 and 75 years; (5) expected hospital treatment duration of $>$ 3 days, with samples collected within 3 days post-SAH; and (6) consent from the patient's close relatives.

The exclusion criteria were as follows: (1) SAH not originating from an aneurysm; (2) a history of stroke-causing neurological deficits such as limb or speech impairments; (3) a history of brain tumors; (4) a history of hematological diseases, such as thrombocytopenia; (5) a recent history of severe infectious diseases; (6) severe liver or kidney dysfunction; (7) pregnancy; and (8) life expectancy less than 1 year due to causes other than the current SAH. All patients received standard medical care during their hospital stay. In addition, there were no requirements regarding the patient's sex, ethnicity, or treatment method.

Ten samples were collected as controls, with the following inclusion criteria: (1) aged 18–75 years; (2) healthy volunteers; and (3) consent signed by the subject or their close relatives. After 3–5 mL of blood was collected *via* a vacuum blood collection tube, the blood cells were collected for subsequent analysis.

GEO Analysis of WNK1 Expression Changes in SAH Mice

Preprocessed RNA-seq transcriptome data from the hippocampi of SAH and control group *Mus musculus* were collected from the Gene Expression Omnibus (GEO) database (GSE167110). Differential RNA-seq transcriptome datasets between the two groups were compared and analyzed to construct a list of differentially expressed genes (DEGs) *via* R Studio. A *P* value $<$ 0.05 and $|\text{fold-change (FC)}| <$ 1 are used as thresholds for analysis, and differences in WNK1 expression levels between the two datasets were calculated.

Animals

Male Sprague-Dawley rats (280 ± 30 g) and BALB/c mice (25–27 g) were purchased from Yangzhou University Experimental Animal Center. The animals were acclimatized for one week at 20–25°C and 50–70% humidity and were given frequent access to water and food.

SAH Rat Model Construction

The rats ($n = 165$) were assigned to 6 groups: a sham surgery group ($n = 15$) and five internal carotid artery puncture SAH groups at various time points within 48 h ($n = 30$ /group). After anesthesia, the rats were placed in a supine position, and the neck skin was incised to separate the common carotid artery, external carotid artery, and internal carotid artery. A filament (Beijing Xinong Technology Co., Ltd, 2626-20A2, Beijing, China) was inserted from the left external carotid artery into the internal carotid artery and advanced forwards until resistance was met to puncture the vessel. The external carotid artery was quickly ligated, and the wound was sutured. Sham surgery rats underwent a similar procedure without puncturing the vessel. Rats in the SAH groups were euthanized at various time points within 48 h post-procedure to collect complete brain tissue. The brain tissue of the sham surgery group was collected 24 h post-procedure. No rats in the sham group died before euthanasia. In the SAH groups, 6 rats died within 3 h, 7 rats died between 6 and 12 h, and 8 rats died within 24 h, with no deaths occurring after 24 h (Supplementary Fig. S1A).

Mice Adeno-Associated Virus (AAV)-WNK1 Transfection

For WNK1 overexpression, pAAV-CX3CR1-WNK1-T2A-ZsGreen virus (AAV-WNK1, 1.8×10^{12} vg/mL) was packaged by HANBIO (Shanghai, China). After the mice were anesthetized, they were fixed onto a ZH-Blue Star C/S Digital Brain Stereotaxic Instrument (Anhui Zhenghua Biological Instrument Equipment Co., Ltd. Anhui, China). The medial prefrontal cortex region of the right lateral ventricle was injected with 1 μ L of AAV-WNK1 at a rate of 0.1 μ L/min for 10 min (AP = +1.78, ML = 0.30, DV = 2.65 mm). Equivalent amounts of saline were injected into the control. SAH modelling was conducted 3 weeks after the AAV-WNK1 injection. Each group contained 15 mice.

Neurological Scoring

Neurological functions were evaluated using the modified Garcia scoring system [24, 25]. This test includes six sensorimotor tasks: spontaneous activity, symmetry of limb movements, forepaw stretching, climbing, proprioception, and

response to vibrissal touch. Scores for each test range from 0 to 3, with the total score (0–18) indicating the extent of neurological deficit. Specifically, higher scores represent less impairment. As shown in Supplementary Fig. S1B, sham rats displayed good neurological function, whereas longer durations post-SAH within 12 h correlated with more severe neurological deterioration.

Brain Water Content Measurement

The animals were euthanized at 24 h post-SAH, and their brains were weighed (wet weight). After drying at 80°C for 48 h, the dry weights of the brains were recorded. The water content was calculated as follows: (wet weight – dry weight)/wet weight $\times 100\%$.

H&E Staining

The cortical and hippocampal regions were fixed in a fixative solution at ten times their volume for 12 h. The paraffin-embedded tissue was cut into 3–5 μ m sections, dewaxed in xylene, dehydrated in gradient alcohol, and stained with H&E. Tissue morphology was observed blindly and assessed by pathologists for typical pathological changes.

Nissl Staining

After thorough dewaxing of the paraffin sections, 0.5% cresyl violet (Beyotime, Beijing, China) was applied to cover the entire sample, which was subsequently stained for 10 min. The sections were differentiated in a 0.25% acetic acid ethanol solution for a few seconds, dehydrated in absolute ethanol, and cleared in xylene. Finally, the extent of neuronal damage was assessed under a microscope.

Cell Culture, Transfection, and Stimulation

BV-2 cells were cultured in DMEM, Cl^- -free DMEM (145 mmol/L NaGluconate, 5 mmol/L KGluconate), or DMEM with additional KCl (100 mmol/L) at 37°C and 5% CO_2 . All media were supplemented with 10% serum and 1% penicillin–streptomycin. BV-2 cells were incubated with hemin (51280, purity 96%, Sigma–Aldrich, St. Louis, MO, USA) at concentrations within 800 μ mol/L for 24 h [13]. Cell viability and inflammation levels were measured using CCK-8 and NO assay kits at 450 nm and 540 nm, respectively.

Following the manufacturer's instructions, Lipofectamine 6000 reagent (C0526, Beyotime) was used to transfect BV-2 cells with WNK1 plasmid (TFORF1892, 144315, Addgene, Watertown, MA, USA) and P2X7R (Pcmv-p2rx7 (mouse)-HA, Miaoling, Shanghai, China). At 48 h post-transfection, the cells were stimulated with 200 μ mol/L hemin for 24 h. The transfection efficiency was verified by Western blotting.

ELISA

Blood was collected and centrifuged to separate the serum. The levels of the inflammatory cytokines IL-1 β (88-6010A-22, 88-7013-22, Invitrogen, Carlsbad, CA, USA), IL-6 (88-50625-22, 88-7064-88, Invitrogen), and TNF- α (88-7340-22, 88-7324-88, Invitrogen) and LDH release (A020-2-2, Nanjing Jiancheng) in the serum and BV-2 cell supernatant were measured using ELISA kits per the manufacturers' instructions. Cytokine concentrations were calculated using each standard curve provided.

K⁺ and Cl⁻ Measurements

Following the manufacturer's protocol, potassium and chloride ion concentrations in BV-2 cells were determined *via* a K⁺ assay kit (C001-2-1, Nanjing Jiancheng, Nanjing, China) and a Cl⁻ assay kit (C003-2-1, Nanjing Jiancheng). BV-2 cells were resuspended in PBS. After counting, cells were centrifuged at 2000 rpm for 10 min to collect the pellet. Then, 0.3 mL of deionized water was added, the cells were sonicated in an ice bath, and the supernatant was collected. To each 10- μ L aliquot of the supernatant, 250 μ L of mercuric thiocyanate reagent was added. The mixture was incubated at 37°C for 2 min before the optical density (OD) value was measured at a wavelength of 505 nm. A standard curve was constructed using a Cl⁻ standard solution to calculate the chloride ion content in the BV-2 cells. To determine the potassium ion content, 50 μ L of the supernatant was removed. Then, 200 μ L of NA-TPB (sodium tetraphenylborate) detection reagent working solution was added, and the mixture was allowed to react for 5 min. The OD was measured at 440 nm. A standard curve was constructed using a K⁺ standard solution to calculate the potassium ion content in the BV-2 cells.

Immunofluorescence

The brain sections were permeabilized in 0.2% Triton X-100, and were reacted with anti-WNK1 (K003426P, 1:200, Solabio, Beijing), anti-Iba1 (GB12105-100, 1:2000, Servicebio, Nanjing), anti-CD86 (WL05184, 1:500, Wanlei, Shenyang, China), anti-CD206 (WL06177, 1:500, Wanlei), and anti-ASC (WL02462, 1:200, Wanlei) antibodies overnight. CY3-conjugated goat anti-rabbit IgG (SA00009-2, 1:100, Proteintech, Wuhan, China) or FITC-conjugated goat anti-mouse or rabbit IgG (SA00003-1, SA00003-2, 1:500, Proteintech, Wuhan) was used to detect the primary antibodies after incubation for 1 h at 37°C in the dark. Nuclei were stained with DAPI (2 μ g/mL) at room temperature for 5 min. WNK1 and IBA1 localization and ASC oligomerization were observed under a confocal microscope.

For the ASC oligomerization analysis, the negative ASC signal was a diffuse red signal, whereas the activated ASC (ASC speck) was in a spot-like aggregation in the brain tissue or cell. The percentage of ASC specks was calculated as ASC spot-like aggregation cell number/total cell number \times 100%.

Immunohistochemistry

In accordance with the instructions of the M&R HRP/DAB detection IHC kit (HC301, Vazyme, Nanjing), after dewaxing, the cerebral cortex or hippocampus tissue sections were subjected to antigen retrieval and blocking of endogenous peroxidases, followed by incubation with WNK1 antibody (K114216P; 1:50, Solabio) overnight. HRP-conjugated polymers were incubated at 37°C for 20 min. The sections were then stained with DAB solution, counterstained with hematoxylin, and mounted with glycerol. WNK1 protein expression levels in the rat cerebral cortex or hippocampus were blindly evaluated under an optical microscope.

RT-qPCR

RNA was extracted from samples of the cerebral cortex, hippocampus, and BV-2 cells *via* RNA isolation reagent (R401-01, Vazyme). Genomic DNA contamination was removed, and cDNA was synthesized *via* RTIII Mix (RN05010, Monad, Wuhan). RT-qPCR was applied *via* 10-fold dilution of the cDNA and SYBR Green qPCR mix (RN04004, Monad) with specific primers to amplify target genes. The mRNA content was calculated using the 2^{- $\Delta\Delta$ CT} method. The primer sequences are provided in Table S1 [26].

Western blotting

Proteins from brain tissues or cells were prepared using RIPA buffer containing PMSF according to the manufacturer's instructions. Blood samples did not require pretreatment. Proteins from the BV-2 supernatant were extracted with chloroform and methanol and dissolved in 1% SDS buffer. Protein was subsequently quantified using a BCA kit. Proteins (20 μ g) were separated *via* electrophoresis and transferred to a PVDF membrane. The membrane was reacted with caspase-1 (AG-20B-0042-C100, 1:1000, Adipogen), P2X7R (A10511, 1:500, ABclonal, Wuhan), NLRP3 (A24294, 1:1000, ABclonal), IL-1 β (A16288, 1:1000, ABclonal), WNK1 (K003426P, 1:1000, Solabio), GAPDH (81640-5-RR, 1:5000, Sangon Biotech, Shanghai), beta actin (20536-1-AP, 1:5000, Proteintech), HRP-conjugated goat anti-rabbit (BA1054, 1:5000, Boster, Wuhan) and goat

anti-mouse (BA1075, 1:5000, Boster) antibodies. The membrane was developed *via* an enhanced chemiluminescence solution (E422-01, Vazyme) and imaged *via* a multifunctional hypersensitive imaging system.

Open Field Test

The animals were gently placed in the experimental box and allowed to explore freely for 5 min. The box was cleaned with 70% ethanol between each experiment. Locomotor activity was measured based on distance traveled and speed to assess spontaneous mobility [27].

Water Maze Test

Navigation tests were conducted for the first three days, followed by a platform recognition test on the fourth day. The animals were released from designated points in the pool facing the wall, and their escape latency (time taken to find the fixed platform) was recorded. If they failed to find the platform within 60 s, they were guided to the platform. On the fourth day, the time and speed at which the platform was located were recorded [27].

Elevated Plus Maze

The animals were gently placed in a closed arm and allowed to explore freely for 5 min. Their movements in the closed arms, open arms, and center area were recorded using video equipment to measure the distance traveled and speed [28].

Statistical Analysis

The data were confirmed to be normally distributed *via* normality tests with GraphPad Prism 9 software *via* the Shapiro–Wilk test, processed *via* one- or two-way ANOVA or unpaired *t*-test for plotting, and expressed as the mean \pm SEM. All the data were subjected to Tukey's *post hoc* analysis. Each result was repeated in three or six separate experiments. * $P < 0.05$, ** $P < 0.01$, and *** $P < 0.001$, ns, no significant difference.

Results

Low WNK1 Expression in SAH

WNK1 is a serine/threonine protein kinase. It has been reported that WNK1 exerts neuroprotective effects by regulating neuroinflammatory responses, influencing the central nervous system. Especially, blood WNK1 plays an important role in regulating blood pressure and ion homeostasis. In clinically collected blood cells from SAH patients, WNK1

protein levels were lower than those in control blood cells (Fig. 1A). Volcano plot analysis of the SAH mouse dataset GSE167110 from the GEO database revealed the downregulation of WNK1 transcription levels (Fig. 1B). Subsequently, we established an SAH rat model and a sham control group model. Western blotting revealed high WNK1 expression in the cortical regions of rats from the sham group, whereas WNK1 expression was suppressed from 3–12 h post-SAH, with levels recovering after 24 h (Fig. 1C). The immunohistochemistry results for WNK1 in the cortex and hippocampus of the rats at 12 h post-SAH also revealed a similar trend (Fig. 1D, E). In addition, we utilized immunofluorescence to detect WNK1 fluorescence signals. In the cortex of sham group rats, Iba1 was expressed at low levels, whereas WNK1 was highly expressed. In contrast, 12 h after SAH, the green fluorescence signal intensity of Iba1 increased, whereas the red fluorescence signal intensity of WNK1 decreased (Fig. 1F, G). Furthermore, we used hemin to induce damage in BV-2 cells to establish an *in vitro* SAH model. BV-2 cells were exposed to various hemin concentrations (25–800 $\mu\text{mol/L}$) for 24 h. Cell viability and inflammation levels were assessed *via* the CCK8 assay, and NO content measurements were made (Supplementary Fig. S2A, B). Hemin increased inflammation and cell death with increasing concentrations. An *in vitro* SAH model was subsequently constructed using 200 $\mu\text{mol/L}$ hemin. The *in vitro* and *in vivo* results were consistent (Fig. 1H, I). These data indicate that WNK1 expression is suppressed after SAH.

WNK1 Inhibits Neurological Deficits and Neuroinflammation Induced by SAH

To further study the function of WNK1 in SAH, we utilized adenoviral vectors carrying WNK1 for overexpression in mice (Supplementary Fig. S3A, B). Initially, full-brain images showed that mice injected with AAV-WNK1 and then subjected to SAH surgery presented significantly reduced brain hemorrhage (Fig. 2A). At 24 h post-SAH, the brain water content was significantly greater than that in the sham group; however, the brain water content of SAH model mice injected with AAV-WNK1 was significantly different from that of SAH model mice (Fig. 2B). Nissl staining revealed that SAH mice presented structural damage to the hippocampus and a significant reduction in the number of cortical neurons compared with sham mice, whereas SAH mice overexpressing WNK1 presented a restored hippocampal structure and an increased number of cortical neurons (Fig. 2C). To assess the extent of neurological dysfunction, open field, water maze, and elevated plus maze tests were also conducted on the sham, SAH, and SAH+AAV-WNK1 groups. Initially, in the open field test, all three groups of mice displayed normal spontaneous activity behaviors, with no significant differences in total distance moved (Fig. 2D,

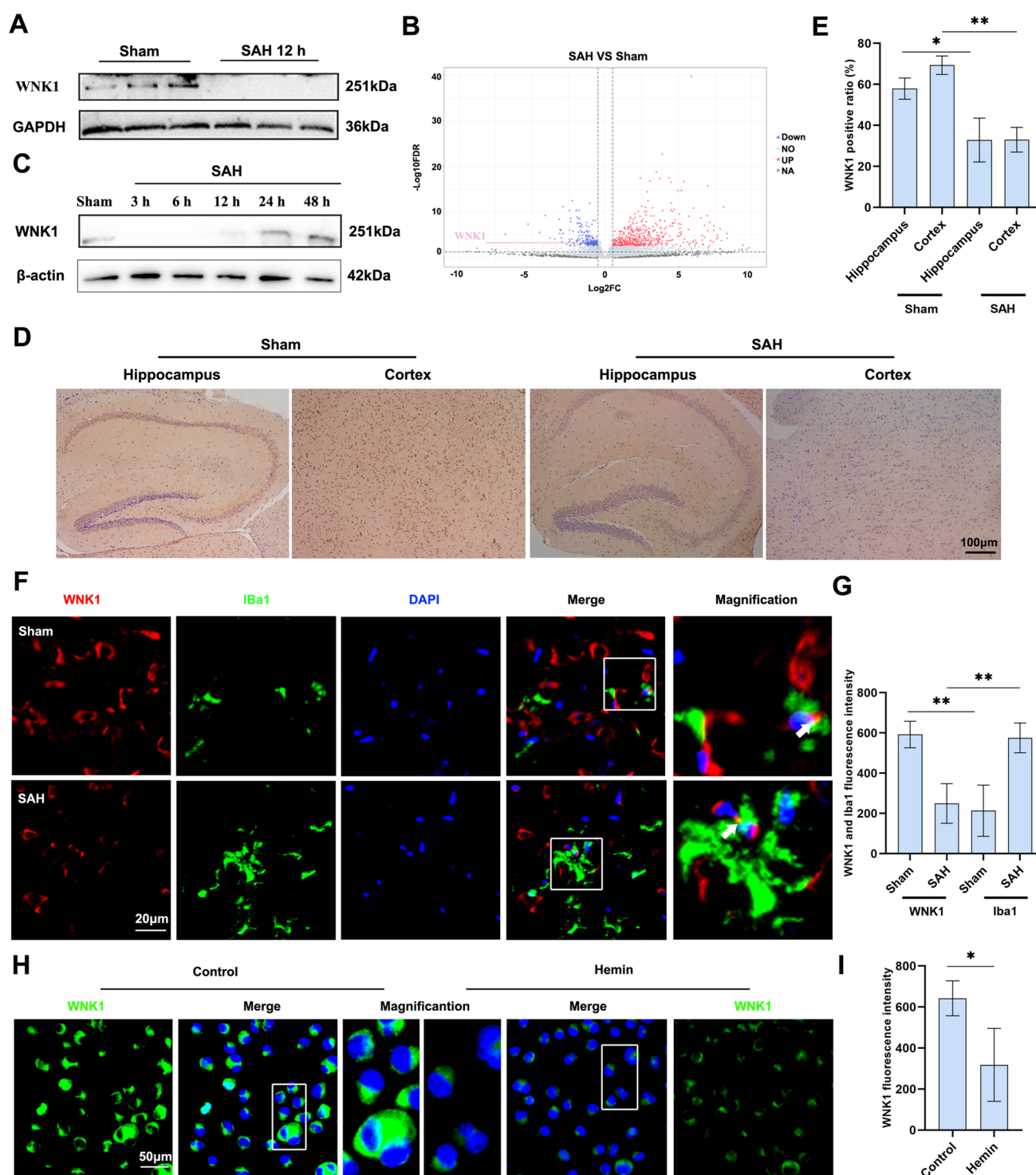
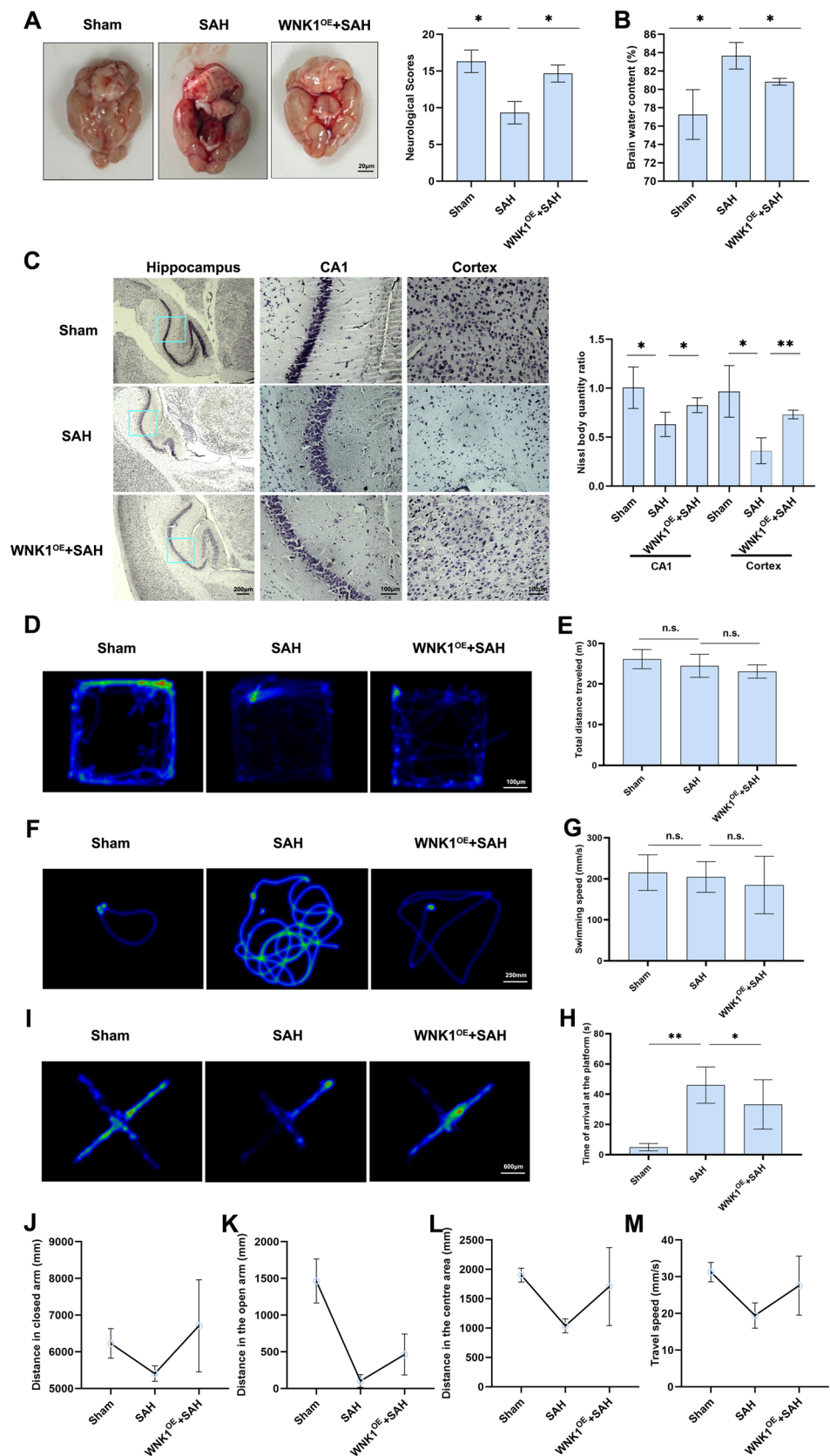


Fig. 1 Low expression of WNK1 in SAH. **A** Expression of WNK1 in blood cells of SAH patients and controls. **B** Volcano plot of DEGs in the hippocampus of SAH and sham mice from the GSE167110 dataset. **C** Western blots of WNK1 protein levels in the rat cerebral cortex at different time points post-SAH. **D**, **E** Immunohistochemical detection of WNK1 protein expression and statistical analysis of the WNK1-positive ratio in the left hemisphere (cortex and hippocampus) of rats 12 h post-SAH ($n = 3$). Scale bar, 100 μm . **F**, **G**

Immunofluorescence detection of WNK1 (red) and Iba1 (green) fluorescence signals in the rat cortex ($n = 3$). White arrow, the co-location of WNK1 and Iba1. Scale bar, 20 μm . **H**, **I** Immunofluorescence detection of WNK1 (green) fluorescence signals in BV-2 stimulated by hemin ($n = 3$). Scale bar, 50 μm . Data are presented as the mean \pm SEM. * $P < 0.05$, ** $P < 0.01$, **** $P < 0.0001$, two-way ANOVA with Tukey's post hoc analysis (**E**, **G**) or unpaired t -test (**I**).

Fig. 2 Overexpression of WNK1 Alleviates Brain Injury Post-SAH. **A** Whole brain images of mice. Scale bar, 20 μ m. **B** Brain water content of mice ($n = 6$). **C** Nissl staining of the mouse cortex, CA1 region (200 \times magnification), and the whole hippocampus ($n = 3$). Scale bars, 200 or 100 μ m. **D** Mouse trajectories in the open field test. Scale bar, 100 μ m. **E** Total distance moved in the open field test ($n = 6$). **F** Trace plot of the mouse in the water maze. Scale bar, 250 μ m. **G** Swimming speed in the water maze ($n = 6$). **H** Latency in the water maze ($n = 6$). **I** Trace in the elevated plus maze. Scale bar, 600 μ m. **J** Distance traveled in the closed arms ($n = 6$). **K** Distance traveled in the open arms ($n = 6$). **L** Distance traveled in the center area ($n = 6$). **M** Travel speed in the elevated plus maze ($n = 6$). Data are presented as the mean \pm SEM. * $P < 0.05$, ** $P < 0.01$, *** $P < 0.0001$, one-way ANOVA with Tukey's post hoc analysis (**A**, **B**, **C**, **E**, **G**, **H**).



E). In the water maze test, SAH group mice took longer to find the hidden platform, and some could not find the platform at all. In contrast, WNK1^{OE}+AAV group mice took less time than SAH group mice did, but there was a smaller difference in swimming speed (Fig. 2F–H). In the elevated plus maze, SAH mice spent more time in the closed arms than did the sham mice and spent almost no time in the open arms. SAH mice exhibited poor exercise; however, SAH mice with WNK1 overexpression displayed stronger exploratory and locomotor behaviors than SAH mice (Fig. 2I–M). In summary, WNK1 overexpression can alleviate neurological damage in mice post-SAH.

Previous research has indicated that neuroinflammation is key to causing EBI. The results revealed that the IL-1 β , TNF- α , and IL-6 contents and mRNA levels were significantly lower in SAH model mice treated with AAV-WNK1 than in SAH model mice (Fig. 3A, B). Immunofluorescence staining revealed increased expression of activated M1-type microglia marked by CD86 in the cortex and decreased expression of activated M2-type microglia marked by CD206 after SAH. In contrast, in the cortex of mice in the WNK1OE+SAH group, activation of M1-type microglia was inhibited, and activation of M2-type microglia was increased (Fig. 3C–E). H&E was used to observe the left hippocampus and cerebral cortex (Fig. 3F). In the SAH group, irregular cell morphology and disordered arrangement were found in the CA3, CA1, and dentate gyrus (DG) areas of the hippocampus, along with deeply stained nuclei. Many blood cells and inflammatory infiltrates were found in the cortical areas of SAH mice. In the WNK1^{OE}+SAH group, the cells exhibited a more regular morphology and were more neatly arranged, with fewer blood cells and fewer inflammatory infiltrates.

We subsequently overexpressed WNK1 in a BV-2 cell model stimulated with hemin to investigate the effects of WNK1 on inflammation in SAH *in vitro*. The Western blot results confirmed the successful overexpression of WNK1 protein in BV-2 cells (Fig. 4A). Compared with the group transfected with an empty vector and stimulated with hemin, the WNK1-overexpressing group exhibited a decrease in inflammatory factor secretion (Fig. 4B). The qPCR results revealed a similar trend (Fig. 4C). These data suggest that WNK1 overexpression alleviates inflammation in microglia.

WNK1 Inhibits SAH-mediated NLRP3 Inflammasome Activation

NLRP3 inflammasome activation is crucial for activated microglia. Initially, in the cortex of SAH patients, the NLRP3-related protein and ASC oligomerization levels were significantly greater than those in the sham group. However, in the WNK1-overexpressing (WNK1^{OE}) + SAH group, these proteins were reduced (Fig. 5A–D). Similarly, in the

in vitro SAH model, WNK1 overexpression significantly reduced the levels of NLRP3-related proteins in the cell pellet and/or supernatant (Fig. 5E, F). In addition, the immunofluorescence results revealed almost no ASC oligomerization in the control and hemin + WNK1 groups, whereas clear ASC oligomerization was present in the hemin group (Fig. 5G, H). Moreover, WNK1 overexpression reduced the release of LDH induced by hemin (Fig. 5I). These data suggest that WNK1 inhibits the NLRP3 inflammasome activation induced by SAH.

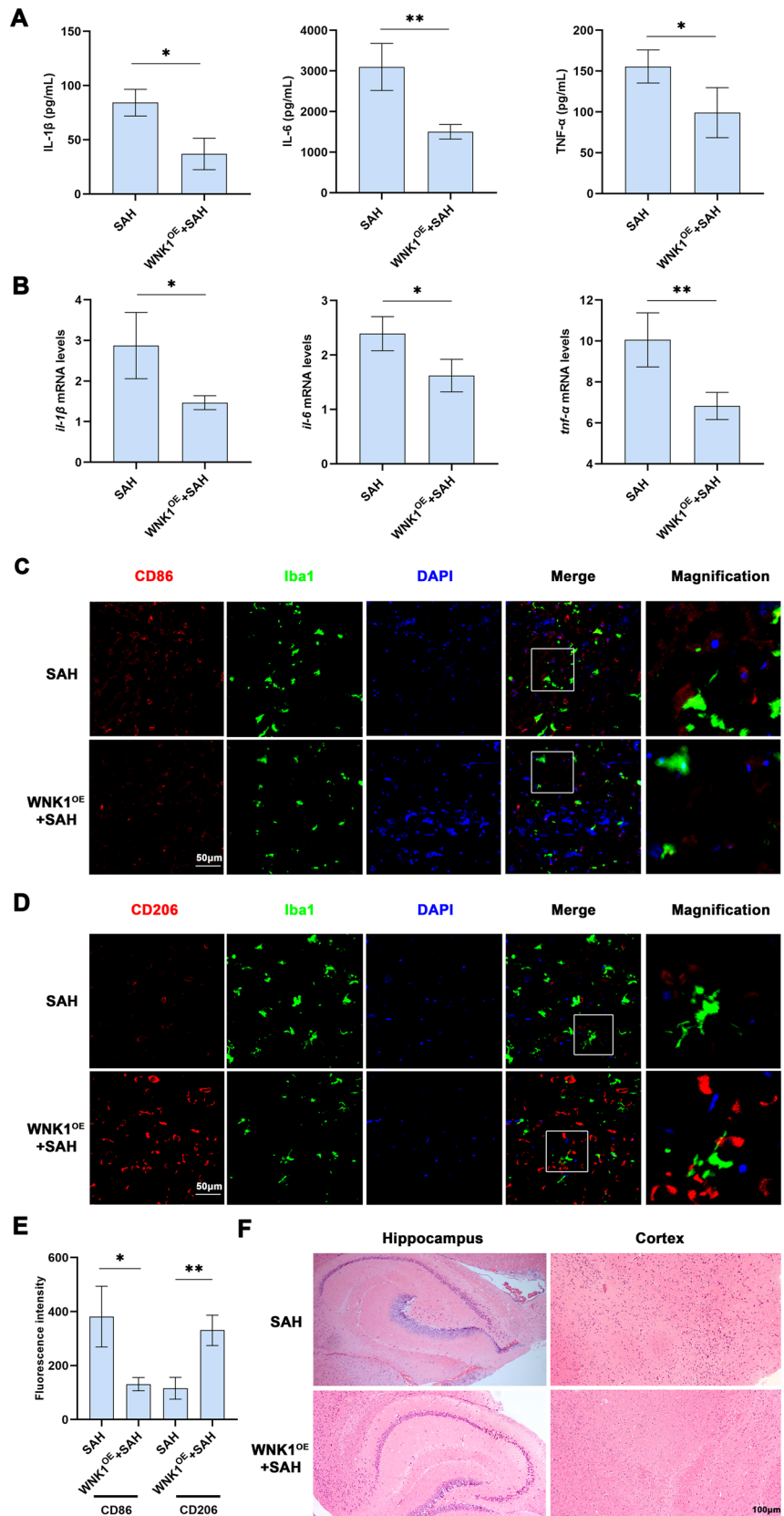
WNK1 Alleviates NLRP3 Inflammasome Activation in a Cl⁻-dependent Manner

Given that WNK1 is an intracellular chloride ion sensor, we next explored how WNK1 inhibits NLRP3 inflammasome activation from an ionic perspective. Compared with unstimulated control BV-2 cells, hemin-stimulated BV-2 cells presented reduced intracellular Cl⁻ and K⁺ levels. In contrast, when WNK1 was overexpressed in BV-2 cells stimulated with hemin, the intracellular Cl⁻ and K⁺ levels increased compared with those in cells stimulated with hemin alone (Fig. 6A, B). BV-2 cells were subsequently cultured under Cl⁻-free conditions. BV-2 cells stimulated with hemin showed significantly higher intracellular NLRP3 and Pro-IL-1 β levels and caspase-1 p20 levels in the culture supernatant compared with non-stimulated cells. WNK1 overexpression in BV-2 cells cultured in Cl⁻-free medium resulted in significantly reduced intracellular NLRP3 and Pro-IL-1 β levels and caspase-1 p20 levels in the culture medium (Fig. 6C, D). Similarly, the results of the immunofluorescence analysis of ASC oligomerization and LDH release followed the same pattern (Fig. 6E–G). These data suggest that WNK1 alleviates NLRP3 inflammasome activation during SAH by inhibiting Cl⁻ efflux.

WNK1 Alleviates P2X7R-induced NLRP3 Inflammasome Activation

Given that P2X7R is a cation channel protein that induces the efflux of ions such as K⁺ and Cl⁻, we explored whether WNK1 can alleviate P2X7R-induced NLRP3 activation. First, the protein immunoblotting results of blood cells from SAH patients revealed that P2X7R protein levels were greater than those in healthy individuals (Fig. 7A). Furthermore, in the blood cells, cerebral cortex, and hippocampus of SAH mice subjected to carotid artery puncture, P2X7R protein levels were greater than those in the sham group and peaked at 24 h post-SAH (Fig. 7B–D). In addition, in BV-2 cells stimulated with hemin *in vitro*, the protein level of P2X7R was greater than that in the control (Fig. 7E), indicating that the P2X7R protein is highly expressed in SAH.

Fig. 3 Overexpression of WNK1 alleviates neuroinflammation in SAH mice. **A** Levels of IL-1 β , TNF- α , and IL-6 in mouse serum ($n = 6$). **B** Levels of mRNA for IL-1 β , TNF- α , and IL-6 in mouse brains ($n = 6$). **C–E** Immunofluorescent detection of CD86 or CD206 (red) and Iba1 (green) fluorescence signals in the cortex ($n = 3$). Scale bar, 50 μ m. **(F)** Histopathological H&E staining of mouse hippocampus and cortex ($n = 3$). Scale bar, 100 μ m. Data are presented as the mean \pm SEM. * $P < 0.05$, ** $P < 0.01$, **** $P < 0.0001$, two-way ANOVA with Tukey's post hoc analysis (**E**) or unpaired t -test (**A**, **B**).



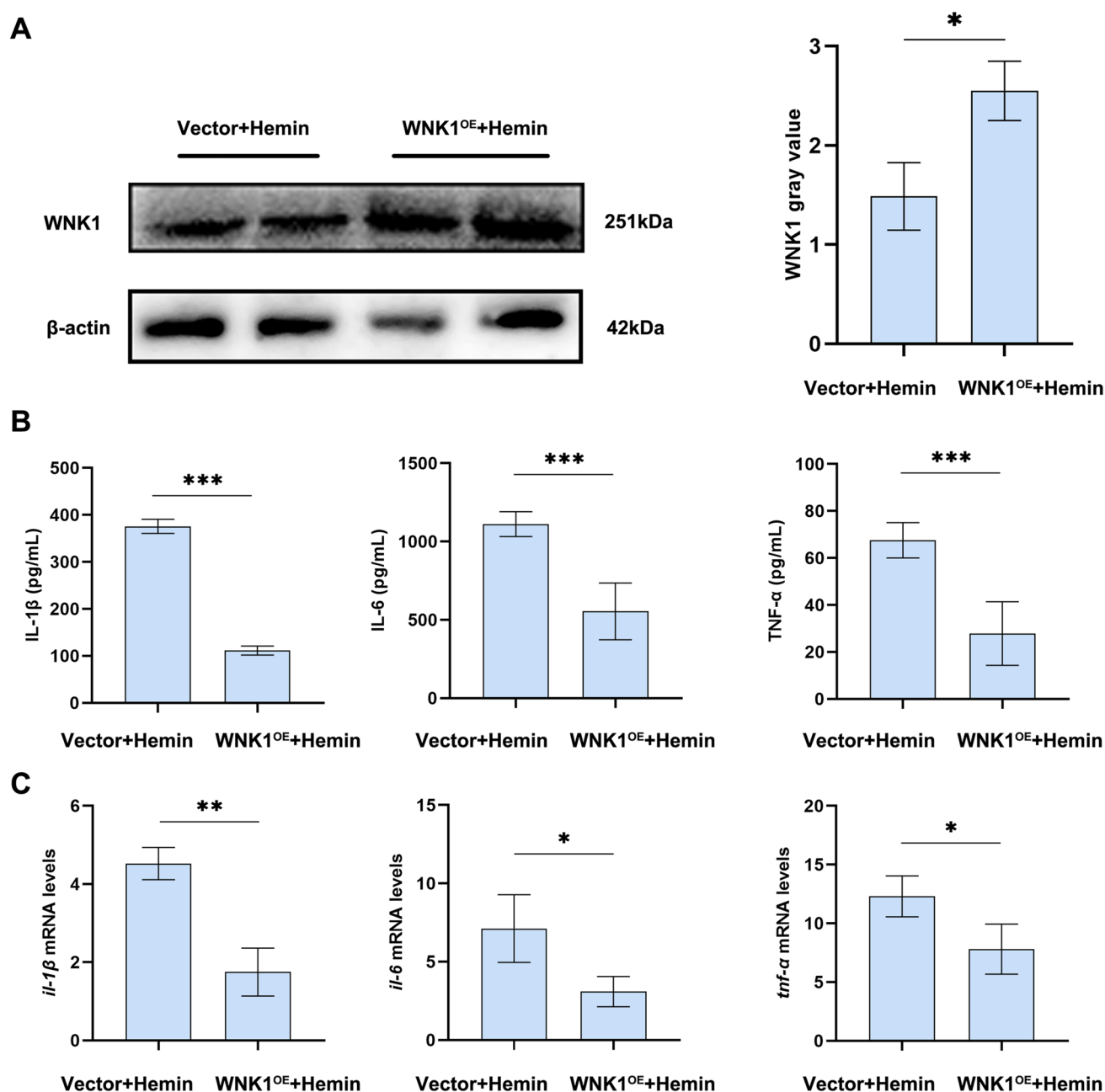


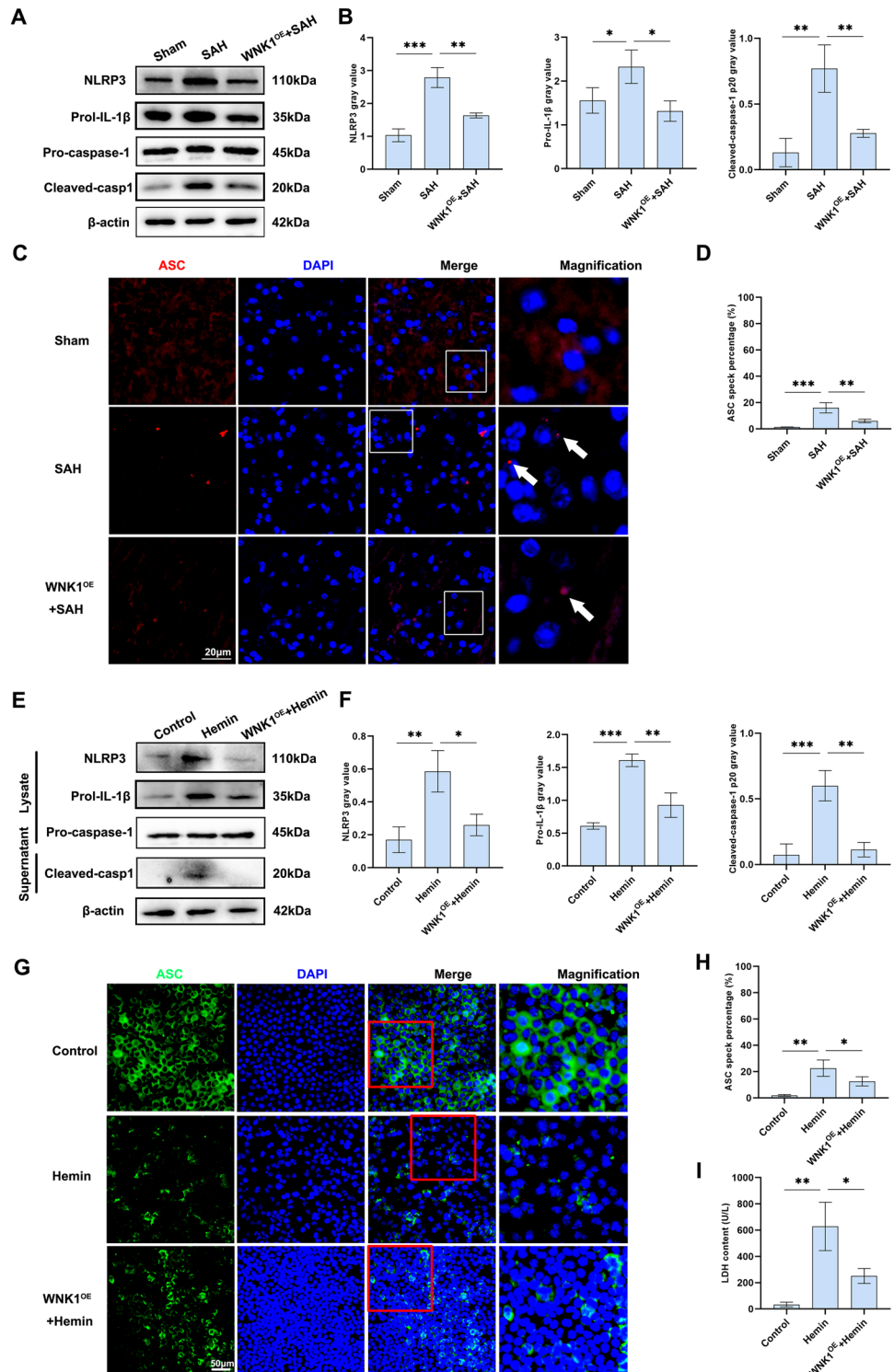
Fig. 4 Overexpression of WNK1 alleviates inflammation in an *in vitro* SAH model. **A** Protein levels of WNK1 in BV-2 cells ($n = 6$). **B** The secretion levels of IL-1β, TNF-α, and IL-6 in the cell super-

natant. **C** The mRNA levels of *IL-1β*, *TNF-α*, and *IL-6* in the cells ($n = 6$). Data are presented as the mean \pm SEM. * $P < 0.05$, ** $P < 0.01$, *** $P < 0.0001$, unpaired *t*-test (A–C).

To further verify whether P2X7R regulates the NLRP3 inflammasome through ion modulation in SAH, P2X7R overexpression and coincubation with KCl were used for reverse validation. First, P2X7R protein overexpression in BV-2 cells transfected with the Pcmv-p2rx7 (mouse)-HA plasmid was confirmed (Supplementary Fig. S4). However,

when incubated with KCl, BV-2 cells presented increased NLRP3 and Pro-IL-1β levels within the cells and increased levels of caspase-1 p20 in the supernatant. However, these elevated levels of key NLRP3 inflammasome proteins were suppressed upon the addition of KCl (Fig. 8A, B). Similarly, the results of the immunofluorescence analysis of

Fig. 5 Overexpression of WNK1 alleviates NLRP3 inflammasome activation in SAH. **A, B** Protein levels and densitometric analysis of NLRP3, Pro-IL-1 β , and caspase-1 p20 in mouse cerebral cortex ($n = 3$). **C, D** Fluorescence and the ratio of ASC specks in the cortex ($n = 3$). White arrow, the activated ASC signal. Scale bar, 20 μ m. **E, F** Protein levels and densitometric analysis of NLRP3, Pro-IL-1 β , and caspase-1 p20 in BV-2 cells ($n = 3$). **G, H** Fluorescence and ratio of ASC specks in BV-2 cells ($n = 3$). Scale bar, 50 μ m. **I** Levels of LDH release in the supernatant of BV-2 cells ($n = 6$). Data are presented as the mean \pm SEM. * $P < 0.05$, ** $P < 0.01$, *** $P < 0.0001$, one-way ANOVA with Tukey's post hoc analysis (**B, D, F, H, I**).



ASC oligomerization and LDH release followed the same pattern (Fig. 8C–E). In summary, P2X7R activates the NLRP3 inflammasome by promoting the efflux of K⁺ and Cl[−] ions in SAH models.

Next, we aimed to determine the relationships among WNK1, P2X7R, and the NLRP3 inflammasome by overexpressing both P2X7R and WNK1 in an SAH *in vitro* model. Compared with P2X7R overexpression alone, WNK1 and

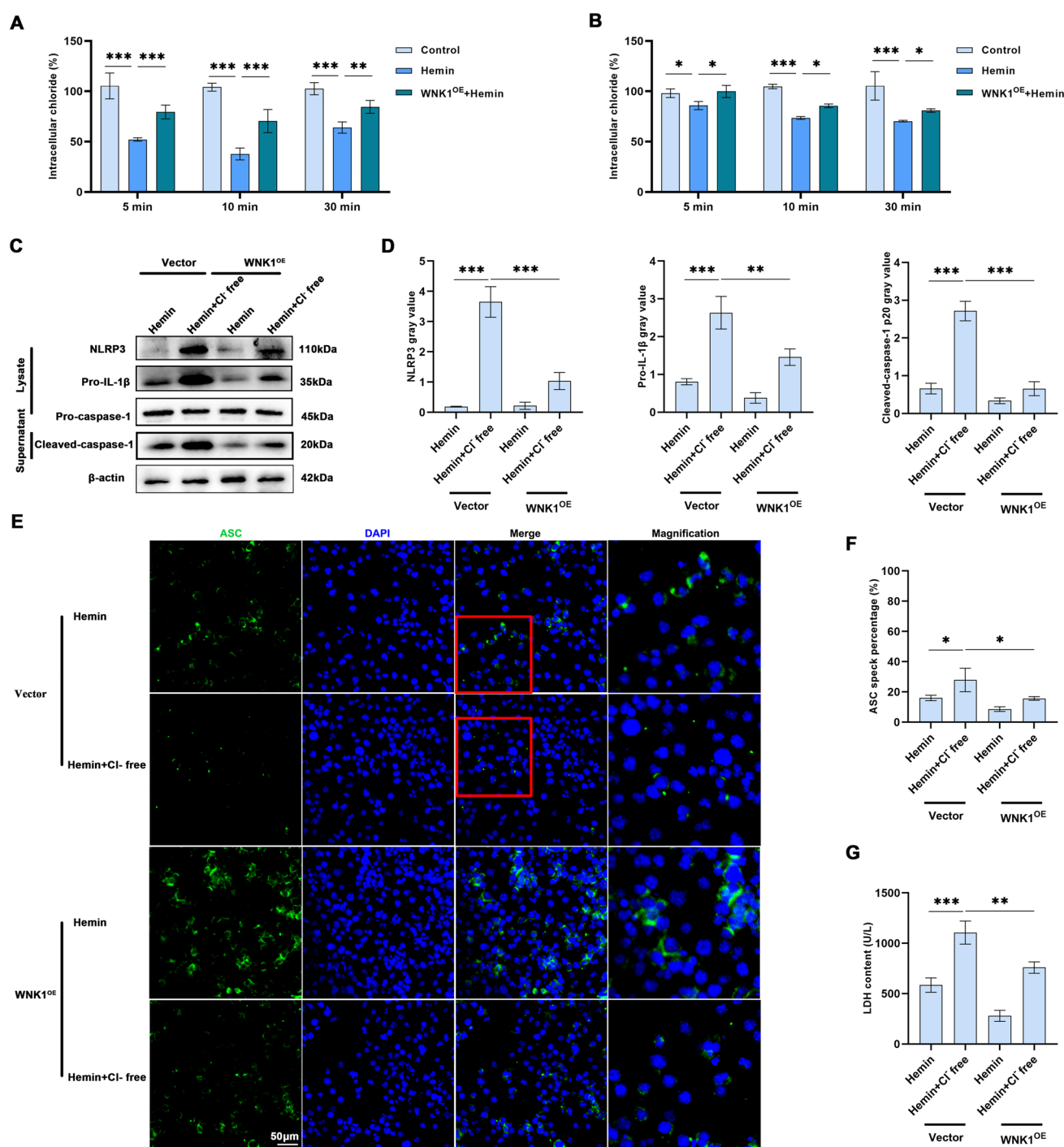


Fig. 6 Cl⁻ free medium counteracts the inhibitory effect of WNK1 on NLRP3 inflammasome activation. **A** Cl⁻ levels in BV-2 cells ($n = 6$). **B** K⁺ levels in BV-2 cells ($n = 6$). **C**, **D** Protein levels of NLRP3, Pro-IL-1β, and caspase-1 p20 in BV-2 cells or culture supernatant ($n = 3$). **E**, **F** Fluorescence and the ratio of ASC specks in BV-2 cells (n

$= 3$). **G** LDH levels in BV-2 cell supernatant ($n = 6$). Scale bar, 50 μm. Data are presented as the mean \pm SEM. * $P < 0.05$, ** $P < 0.01$, *** $P < 0.0001$, one-way (A, B) or two-way ANOVA with Tukey's *post hoc* analysis (D, F, G).

P2X7R co-overexpression significantly reduced NLRP3 and Pro-IL-1β protein levels in BV-2 cells, caspase-1 p20 protein levels in the supernatant of BV-2 cells, ASC oligomerization

in BV-2 cells, and LDH release in the supernatant (Fig. 9). In summary, WNK1 effectively alleviates P2X7R-induced NLRP3 inflammasome activation in SAH.

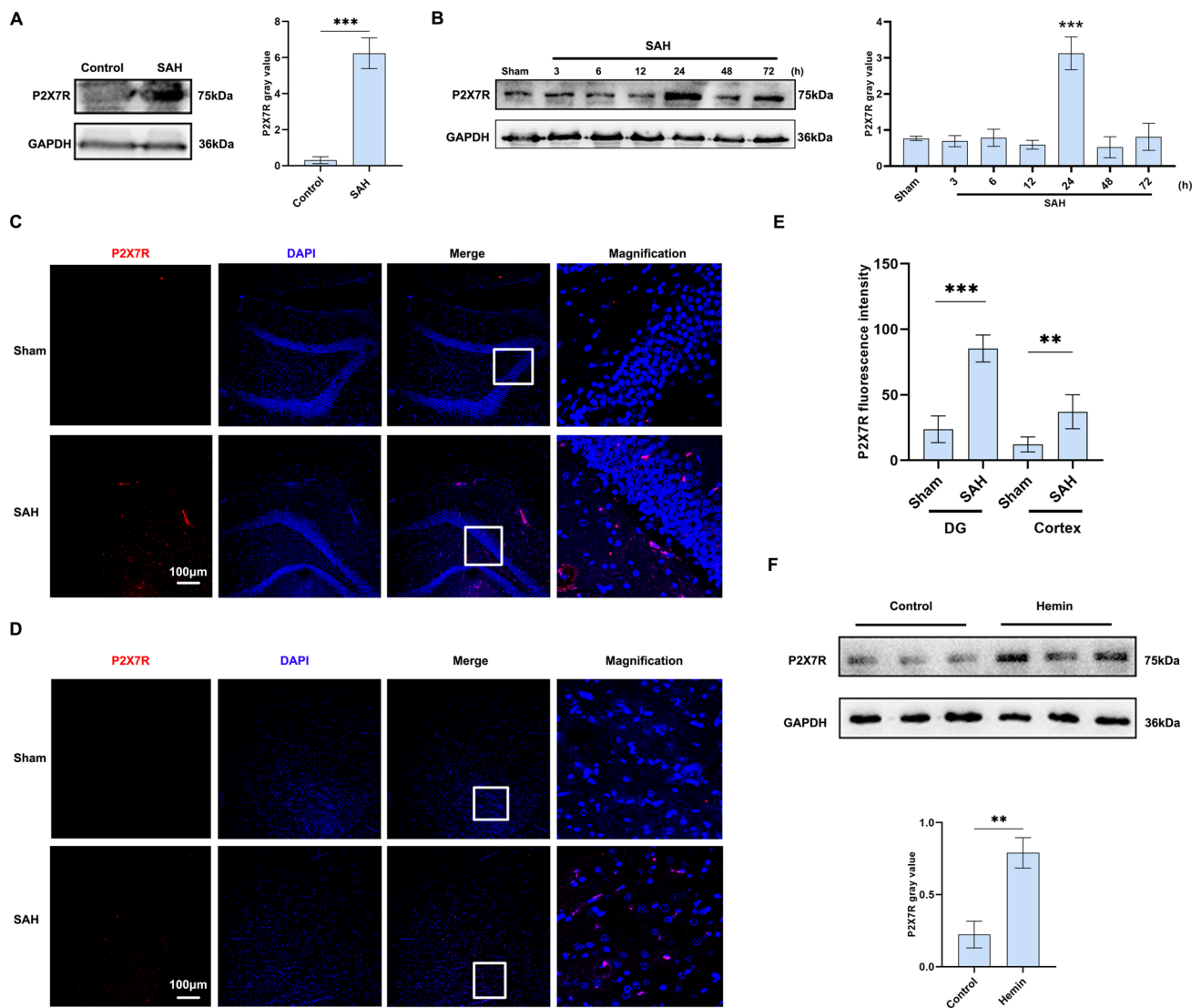


Fig. 7 Increased expression of P2X7R in SAH. **A** Protein levels of P2X7R in the blood of SAH patients ($n = 3$). **B** Protein levels of P2X7R in the blood cells of SAH mice ($n = 3$). **C** Immunofluorescence results of P2X7R in the hippocampus of SAH mice ($n = 3$). **D** Immunofluorescence results of P2X7R in the cerebral cortex of SAH mice ($n = 3$). **E** Immunofluorescence analysis of P2X7R in the hip-

pocampal DG and cerebral cortex of SAH mice ($n = 3$). **F** Protein levels of P2X7R in BV-2 cells stimulated with hemin ($n = 3$). Scale bar, 100 μm . Data are presented as the mean \pm SEM. * $P < 0.05$, ** $P < 0.01$, *** $P < 0.0001$, one-way with Tukey's *post hoc* analysis (**B**, **E**) or unpaired *t*-test (**A**, **F**).

WNK1 Alleviates NLRP3 Inflammasome Activation via OXSR1/STK39

Finally, we explored the specific mechanism by which WNK1 regulates the NLRP3 inflammasome. Inhibitors of OXSR1 (closantel) and STK39 (rafoxanide) were added, and incubation with hemin in WNK1-overexpressing BV-2 cells significantly increased NLRP3 and Pro-IL-1 β protein levels in BV-2 cells, caspase-1 p20 protein levels in the supernatant of BV-2 cells, ASC oligomerization in

BV-2 cells, and LDH release in the supernatant of BV-2 cells (Fig. 10). These data suggest that WNK1 alleviates NLRP3 activation after SAH via the OXSR1/STK39 pathway.

Discussion

In this study, the regulation of EBI and neuroinflammation induced by P2X7R in an SAH model by WNK1 was revealed. WNK1, an intracellular chloride ion sensor, is

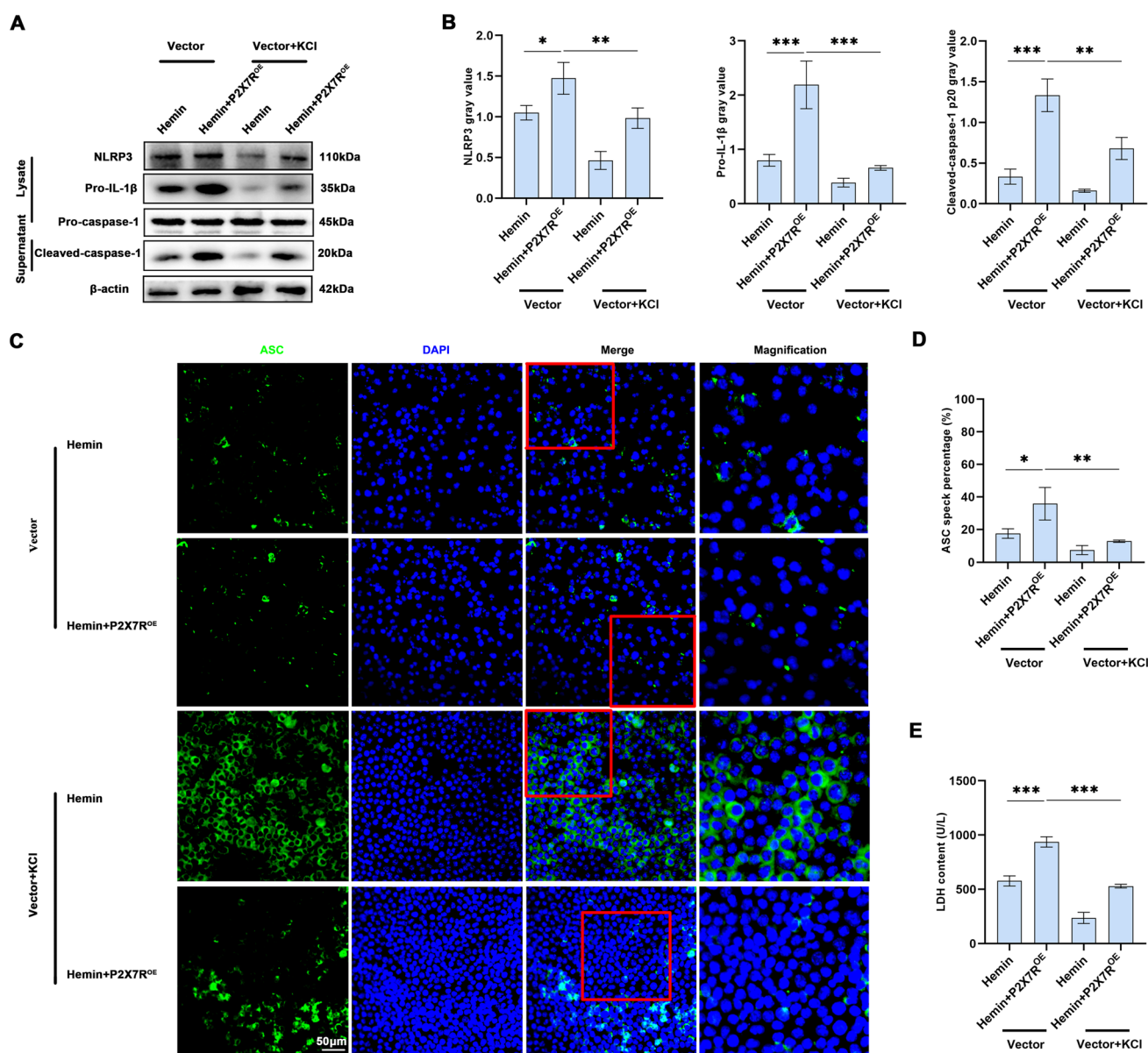


Fig. 8 KCl alleviates P2X7R-induced NLRP3 inflammasome activation. **A**, **B** Protein levels and densitometric analysis of NLRP3, Pro-IL-1 β , and caspase-1 in BV-2 cells or supernatant ($n = 3$). **C** Levels of ASC oligomerization in BV-2 cells. **D** Percentage of ASC specks

in BV-2 cells ($n = 3$). **E** LDH release levels in the supernatant of BV-2 cells ($n = 6$). Scale bar, 50 μ m. Data are presented as the mean \pm SEM. * P < 0.05, ** P < 0.01, *** P < 0.0001, two-way ANOVA with Tukey's post hoc analysis (**B**, **D**, **E**).

significantly reduced during SAH and inhibits the NLRP3 inflammasome in a Cl^- -dependent manner. Furthermore, P2X7R, a cation channel protein, is upregulated in SAH and induces NLRP3 inflammasome activation by regulating K^+ and Cl^- ions. Mechanistically, WNK1 alleviates P2X7R-induced NLRP3 inflammasome activation by maintaining intracellular Cl^- homeostasis through the OXSR1/STK39 signaling pathway. The experimental results of this study provide important medical value and practical significance for the clinical treatment of SAH.

Increasing evidence suggests that the inflammatory response following SAH accelerates EBI post-SAH [29–31]. Microglia are activated in response to acute brain injury [32] and induce cytokines, chemokines, and other immunoregulatory molecules, further exacerbating brain injury [33]. In models of intracerebral hemorrhage, early activation of microglia has been reported, with activated microglia dominating the injury area and worsening brain injury through exacerbation of the inflammatory response [33]. Similarly, microglial activation has been reported in SAH models [9, 33, 34]. In this study, increased IBA1 levels in cortical

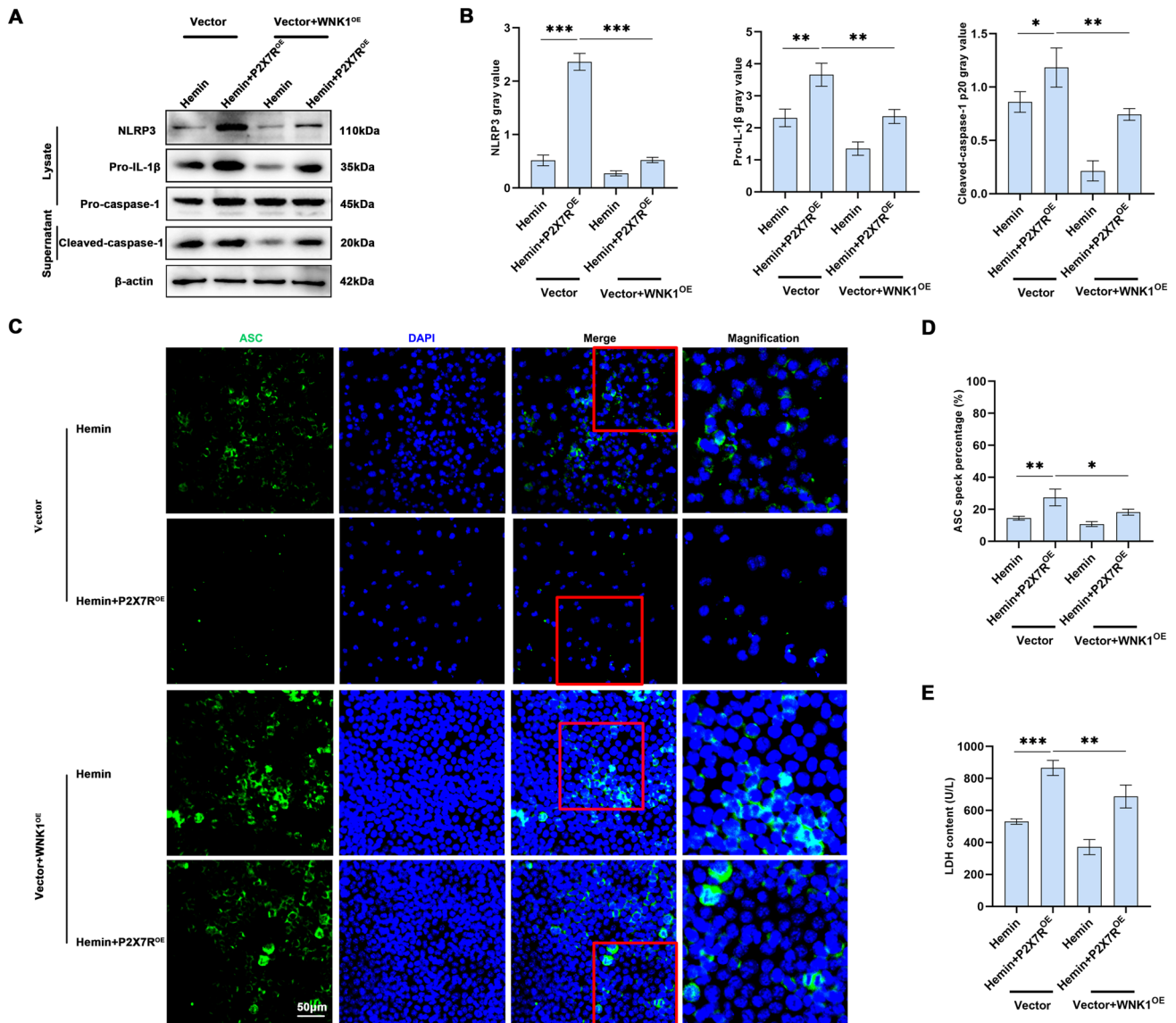


Fig. 9 KCl alleviates P2X7R-induced NLRP3 inflammasome activation. **A**, **B** Protein levels and densitometric analysis of NLRP3, Pro-IL-1 β , and caspase-1 in BV-2 cells or supernatant ($n = 3$). **C** Levels of ASC oligomerization in BV-2 cells. **D** Percentage of ASC specks

in BV-2 cells ($n = 3$). **E** LDH release levels in the supernatant of BV-2 cells ($n = 6$). Scale bar, 50 μ m. Data are presented as the mean \pm SEM. * P < 0.05, ** P < 0.01, *** P < 0.0001, two-way ANOVA with Tukey's *post hoc* analysis (**B**, **D**, **E**).

sections from SAH rats and *in vitro* hemin-stimulated BV-2 cells were found, whereas WNK1 levels decreased as Iba1 increased. Therefore, WNK1 may represent a key target for inhibiting microglial activation and improving EBI and neurological function post-SAH.

In particular, the immunological functions of WNK1 have been widely discussed. WNK1 balances T-cell adhesion and migration [35] and enhances phagocyte clearance of dead cells, eliciting an anti-inflammatory response [36]. WNK1 overexpression resulted in reduced hemorrhage, decreased brain water content, alleviated neuronal damage in the cortex

and hippocampus, and mitigated motor dysfunction. In addition, the proinflammatory factors IL-1 β , IL-6, and TNF- α were downregulated. Similar results were also obtained in the *in vitro* SAH model, where WNK1 overexpression led to reduced inflammatory secretion in the supernatant, decreased mRNA expression of proinflammatory factors within cells, and significantly reduced microglial activation, shifting from the M1 phenotype to the M2 phenotype. Comparable results were reported by Arai *et al.*, where WNK1 knockdown increased the number of LPS-induced cytokines and activated macrophages, indicating that WNK1 may be a

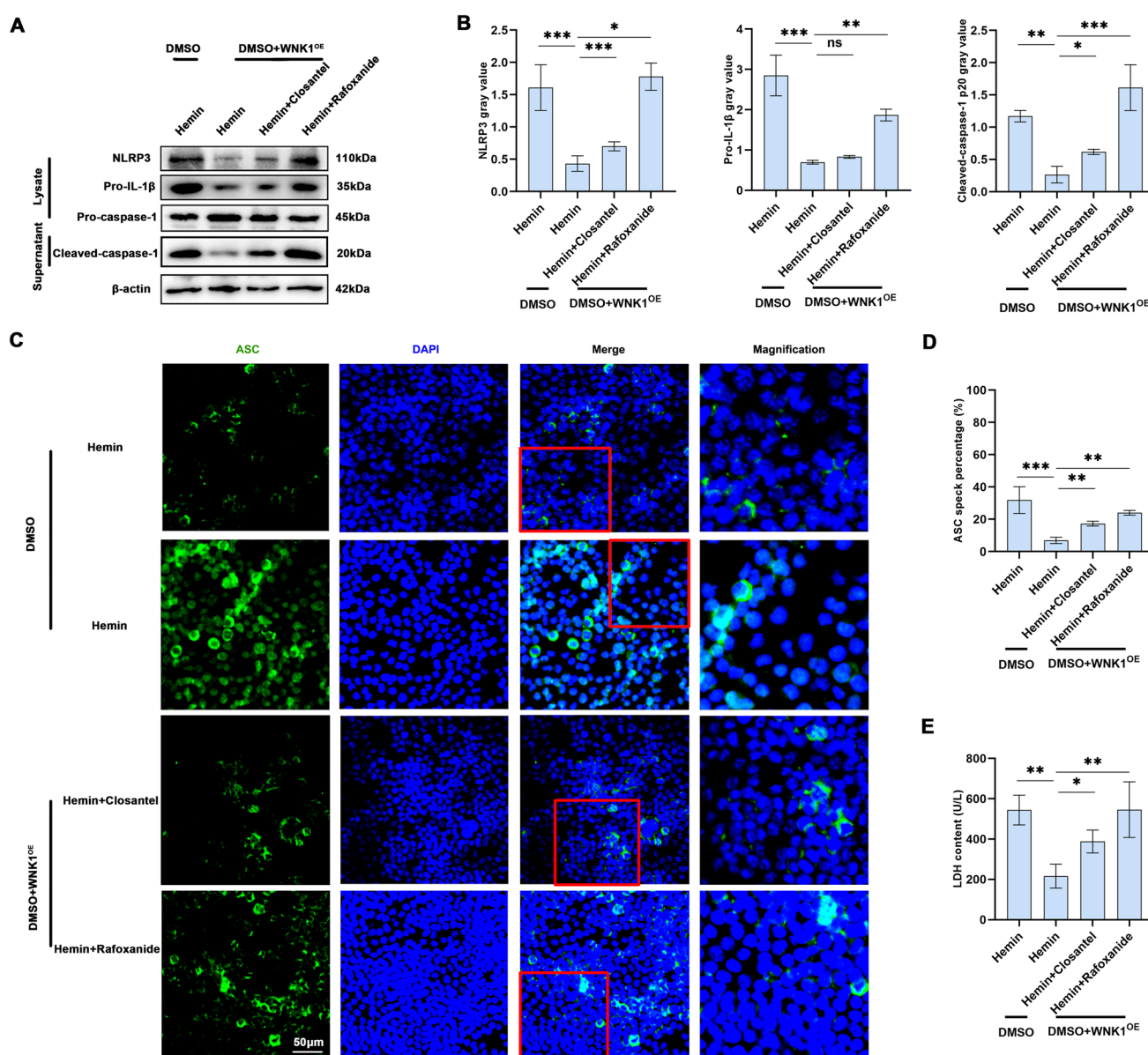


Fig. 10 Inhibition of OXSR1/STK39 reverses the suppression of NLRP3 inflammasome activation by WNK1 overexpression. **A**, **B** Protein levels and densitometric analysis of NLRP3, Pro-IL-1 β , and caspase-1 in BV-2 cells or supernatant ($n = 3$). **C** Levels of ASC oligomerization in BV-2 cells. **D** Percentage of ASC specks in BV-2

cells ($n = 3$). **E** LDH release levels in the supernatant of BV-2 cells ($n = 6$). Scale bar, 50 μ m. Data are presented as the mean \pm SEM. * $P < 0.05$, ** $P < 0.01$, **** $P < 0.0001$, two-way ANOVA with Tukey's post hoc analysis (**B**, **D**, **E**).

target for inflammatory diseases [37]. In conclusion, WNK1 inhibits the neuroinflammatory response following SAH.

The dynamic change in WNK1 expression after SAH initially decreased but then increased within 24 h, which may reflect the complex role of WNK1 in the pathological mechanism of SAH. These results show that the acute stress response of brain tissue after SAH leads to an early decrease in WNK1 expression. This decrease may be related to the inflammatory response and cell injury, which inhibits WNK1 expression, thus affecting the function of ion

channels and further aggravating apoptosis and neuronal injury [38]. At this stage, the cellular response to ischemia and inflammation may lead to changes in the cellular environment, potentially inhibiting WNK1 function, causing ion imbalance, and aggravating the pathological state. However, the increase in WNK1 levels 24 h after the onset of SAH may represent a compensatory response. This change may promote the intracellular balance of sodium and potassium ions by activating intracellular signaling pathways, thereby protecting cells from further damage [39, 40]. Therefore,

further studies will help clarify the specific role of WNK1 in SAH and its regulatory mechanism.

Increasing evidence suggests that NLRP3 participates in microglial activation and induces inflammation [11, 41]. Substantial evidence from SAH studies indicates that NLRP3 is a major contributor to neuroinflammation and that NLRP3 inhibition can improve EBI and delay cerebral vasospasm following SAH [42, 43]. In this study, similar phenomena were found. Specifically, NLRP3 was assembled and activated to trigger caspase-1 activation in both SAH mice and hemin-stimulated microglia. Activated caspase-1 proteolytically processes the proinflammatory cytokine IL-1 β into its active form, thereby amplifying the innate immune system. Therefore, the NLRP3 inflammasome is key to neuroinflammation following SAH. This study further revealed that WNK1 overexpression significantly inhibited NLRP3 in the SAH model, as evidenced by decreased protein expression of NLRP3 and caspase-1 p20 and reduced levels of ASC oligomerization. These findings are consistent with the data from Jiang *et al.*, who reported that WNK1 overexpression significantly inhibits NLRP3 inflammasome formation in bone marrow mesenchymal stem cells [44]. In summary, WNK1 is a target for inhibiting NLRP3 inflammasome activation following SAH.

As a major regulator of intracellular ion homeostasis and cell volume, WNK1 is activated during osmotic stress or when intracellular Cl⁻ levels decrease to maintain the ion balance within the cell. To further determine its function, BV-2 cells were cultured in a Cl⁻-free medium, and WNK1 was overexpressed. NLRP3 inflammasome levels increased in the medium, and the medium counteracted the inhibitory effect of WNK1 on NLRP3 inflammasome activation. The importance of Cl⁻ in NLRP3 inflammasome activation was supported by Lindsey *et al.*, who demonstrated that the Cl⁻ sensor WNK1 negatively regulates Cl⁻ efflux and NLRP3 inflammasome activation [23]. In summary, WNK1 alleviates NLRP3 following SAH by regulating Cl⁻.

Typically, the second signal for NLRP3 inflammasome activation involves three different mechanisms: K⁺ efflux, mitochondrial reactive oxygen species, and lysosomal instability [45]. The P2X7R/NLRP3 inflammasome is an effective target for regulating the inflammatory response following SAH, and blocking the P2X7R/NLRP3 inflammasome (e.g., with BBG, a P2X7R antagonist) exerts potential anti-inflammatory effects in the central nervous system [46]. In this study, BV-2 cell cocubation with P2X7R and KCl also demonstrated this effect; under hemin stimulation, cocubation with P2X7R and KCl effectively alleviated the NLRP3 inflammasome activation induced by P2X7R alone. In summary, P2X7R is an upstream target for NLRP3 inflammasome activation following SAH, which is achieved through

the regulation of intracellular ion efflux. Furthermore, simultaneous overexpression of WNK1 and P2X7R was used to further investigate the mechanism of WNK1 in SAH. The experimental results indicated that WNK1 overexpression also alleviated P2X7R-induced NLRP3 inflammasome activation in the SAH model. These data indicate that WNK1 mitigates P2X7R-induced NLRP3 inflammasome activation under SAH conditions.

After activation, WNK1 kinase phosphorylates STK39 and OXSR1. STK39 and OXSR1 regulate intracellular ion concentrations (Na⁺, K⁺, and Cl⁻) by controlling the activity of SLC12 family Cl⁻ cotransporters [47, 48]. These kinases modulate ion flux by acting on channels responsible for Na⁺/K⁺/Cl⁻ cotransport across the cell membrane [38, 49]. Others have demonstrated that inhibition of NLRP3 inflammasome activation requires the classical WNK1/OXSR1/STK39 kinase signaling pathway *via* pretreatment with two different inhibitors that bind to allosteric sites on the C-terminal domains of the STK39 and OXSR1 kinases [23]. Consistent with their findings, in the SAH model, the inhibition of the WNK1/OXSR1/STK39 signaling pathway using two inhibitors of OXSR1/STK39 (closantel and rafoxanide) resulted in NLRP3 inflammasome activation. In summary, WNK1 inhibits the NLRP3 inflammasome following SAH through the OXSR1/STK39 pathway.

There are several limitations in this study, including the following: (1) Overexpression of WNK1 3 weeks before the SAH model may not accurately reflect the physiological environment after the occurrence of SAH; overexpression of WNK1 does not match the time node of SAH, which may lead to the failure to accurately record its true role in the pathogenesis of SAH. (2) WNK1 overexpression 3 weeks before SAH may induce a series of nonspecific effects, which may have an impact on SAH modelling and thus affect the final experimental results. For example, chronic WNK1 overexpression may alter the intracellular ion balance, leading to unexpected neurocellular responses that obscure the true efficacy of pharmacological interventions. (3) Pharmacological intervention after the occurrence of SAH may be more realistic for simulating clinical treatment. By recording changes in WNK1 expression after SAH, researchers can better understand its role in disease progression. Existing experimental designs do not provide room for such dynamic changes, so the results may underestimate or overestimate the potential effects of WNK1. (4) Overexpression before SAH modelling may lead to long-term or persistent WNK1 expression in brain tissue, but this may not accurately reflect the real situation at the onset of SAH. In general, WNK1-overexpressing models take some time to recover base levels. Moreover, if WNK1 expression is too high, the actual effects of pharmacological intervention may be masked. To address these limitations, pharmacological interventions can be applied after SAH to assess changes in

WNK1 expression levels and their impact on pathophysiology, thus enhancing the clinical reality and evaluating the potential therapeutic utility of WNK1.

Conclusions

In summary, in this study, we demonstrated that WNK1 is crucial for inhibiting neuroinflammation and EBI induced by P2X7R following subarachnoid hemorrhage. Our findings indicate that WNK1 inhibits P2X7R-induced NLRP3 inflammasome activation by sensing intracellular chloride ion reduction and activating the WNK1/OXSR1/STK39 pathway, thereby alleviating neuroinflammation in EBI after SAH. Therefore, WNK1 represents an ideal target in the treatment of SAH.

Acknowledgements This work was supported by Grants from the Basic Research Program of Jiangsu (BK20240492), Lianyungang Science and Technology Plan Project (JCYJ2304), Lianyungang Aging Health Research Project (L202301), and Doctoral Research Start-up Fund of the First People's Hospital of Lianyungang City (BS202314). The funders had no role in study design, data collection and analysis, decision to publish, or preparation of the manuscript.

Conflict of interest The authors declare that they have no conflict of interest.

References

- Moon K, Levitt MR, Almeyty RO, Nakaji P, Albuquerque FC, Zabramski JM. Treatment of ruptured anterior communicating artery aneurysms: Equipoise in the endovascular era? *Neurosurgery* 2015, 77: 566–571.
- Cahill J, Calvert JW, Zhang JH. Mechanisms of early brain injury after subarachnoid hemorrhage. *J Cereb Blood Flow Metab* 2006, 26: 1341–1353.
- Geraghty JR, Davis JL, Testai FD. Neuroinflammation and microvascular dysfunction after experimental subarachnoid hemorrhage: Emerging components of early brain injury related to outcome. *Neurocrit Care* 2019, 31: 373–389.
- Peng J, Pang J, Huang L, Enkhjargal B, Zhang T, Mo J, *et al.* LRP1 activation attenuates white matter injury by modulating microglial polarization through Shc1/PI3K/Akt pathway after subarachnoid hemorrhage in rats. *Redox Biol* 2019, 21: 101121.
- Pang J, Peng J, Matei N, Yang P, Kuai L, Wu Y, *et al.* Apolipoprotein E exerts a whole-brain protective property by promoting M1? Microglia quiescence after experimental subarachnoid hemorrhage in mice. *Transl Stroke Res* 2018, 9: 654–668.
- Suzuki H. Inflammation: A good research target to improve outcomes of poor-grade subarachnoid hemorrhage. *Transl Stroke Res* 2019, 10: 597–600.
- Lu Y, Zhang XS, Zhang ZH, Zhou XM, Gao YY, Liu GJ, *et al.* Peroxiredoxin 2 activates microglia by interacting with Toll-like receptor 4 after subarachnoid hemorrhage. *J Neuroinflammation* 2018, 15: 87.
- Salter MW, Stevens B. Microglia emerge as central players in brain disease. *Nat Med* 2017, 23: 1018–1027.
- Gao YY, Tao T, Wu D, Zhuang Z, Lu Y, Wu LY, *et al.* MFG-E8 attenuates inflammation in subarachnoid hemorrhage by driving microglial M2 polarization. *Exp Neurol* 2021, 336: 113532.
- Zheng ZV, Lyu H, Lam SYE, Lam PK, Poon WS, Wong GKC. The dynamics of microglial polarization reveal the resident neuroinflammatory responses after subarachnoid hemorrhage. *Transl Stroke Res* 2020, 11: 433–449.
- Tao W, Hu Y, Chen Z, Dai Y, Hu Y, Qi M. Magnolol attenuates depressive-like behaviors by polarizing microglia towards the M2 phenotype through the regulation of Nrf2/HO-1/NLRP3 signaling pathway. *Phytomedicine* 2021, 91: 153692.
- Yin D, Zhou S, Xu X, Gao W, Li F, Ma Y, *et al.* Dexmedetomidine attenuated early brain injury in rats with subarachnoid hemorrhage by suppressing the inflammatory response: The TLR4/NF- κ B pathway and the NLRP3 inflammasome may be involved in the mechanism. *Brain Res* 2018, 1698: 1–10.
- Liu C, Yao K, Tian Q, Guo Y, Wang G, He P, *et al.* CXCR4-BTK axis mediate pyroptosis and lipid peroxidation in early brain injury after subarachnoid hemorrhage via NLRP3 inflammasome and NF- κ B pathway. *Redox Biol* 2023, 68: 102960.
- Davalos D, Grutzendler J, Yang G, Kim JV, Zuo Y, Jung S, *et al.* ATP mediates rapid microglial response to local brain injury *in vivo*. *Nat Neurosci* 2005, 8: 752–758.
- McCarthy AE, Yoshioka C, Mansoor SE. Full-length P2X₇ structures reveal how palmitoylation prevents channel desensitization. *Cell* 2019, 179: 659–670.e13.
- He Y, Zeng MY, Yang D, Motro B, Núñez G. NEK7 is an essential mediator of NLRP3 activation downstream of potassium efflux. *Nature* 2016, 530: 354–357.
- Kelley N, Jeltema D, Duan Y, He Y. The NLRP3 inflammasome: An overview of mechanisms of activation and regulation. *Int J Mol Sci* 2019, 20: 3328.
- Man SM, Kanneganti TD. Regulation of inflammasome activation. *Immunol Rev* 2015, 265: 6–21.
- Richardson C, Alessi DR. The regulation of salt transport and blood pressure by the WNK-SPAK/OSR1 signalling pathway. *J Cell Sci* 2008, 121: 3293–3304.
- Wang X, Finegan KG, Robinson AC, Knowles L, Khosravi-Far R, Hinchliffe KA, *et al.* Activation of extracellular signal-regulated protein kinase 5 downregulates FasL upon osmotic stress. *Cell Death Differ* 2006, 13: 2099–2108.
- Anselmo AN, Earnest S, Chen W, Juang YC, Kim SC, Zhao Y, *et al.* WNK1 and OSR1 regulate the Na⁺, K⁺, 2Cl⁻ cotransporter in HeLa cells. *Proc Natl Acad Sci USA* 2006, 103: 10883–10888.
- Richardson C, Rafiqi FH, Karlsson HKR, Moleleki N, Vandewalle A, Campbell DG, *et al.* Activation of the thiazide-sensitive Na⁺-cl⁻ cotransporter by the WNK-regulated kinases SPAK and OSR1. *J Cell Sci* 2008, 121: 675–684.
- Mayes-Hopfinger L, Enache A, Xie J, Huang CL, Köchl R, Tybulewicz VLJ, *et al.* Chloride sensing by WNK1 regulates NLRP3 inflammasome activation and pyroptosis. *Nat Commun* 2021, 12: 4546.
- Feng L, Chen Y, Ding R, Fu Z, Yang S, Deng X, *et al.* P2X7R blockade prevents NLRP3 inflammasome activation and brain injury in a rat model of intracerebral hemorrhage: Involvement of peroxynitrite. *J Neuroinflammation* 2015, 12: 190.
- Matsumura K, Peeyush Kumar T, Guddanti T, Yan Y, Blackburn SL, McBride DW. Neurobehavioral deficits after subarachnoid hemorrhage in mice: Sensitivity analysis and development of a new composite score. *J Am Heart Assoc* 2019, 8: e011699.
- Zhao P, Li X, Yang Q, Lu Y, Wang G, Yang H, *et al.* Malvidin alleviates mitochondrial dysfunction and ROS accumulation through activating AMPK- α /UCP2 axis, thereby resisting inflammation and apoptosis in SAE mice. *Front Pharmacol* 2023, 13: 1038802.

27. Xu D, Liu J, Meng S, Sun M, Chen Y, Hong Y. Isoflurane-induced neuroinflammation and NKCC1/KCC2 dysregulation result in long-term cognitive disorder in neonatal mice. *BMC Anesthesiol* 2024, 24: 200.
28. Zhang H, Wang L, Wang X, Deng L, He B, Yi X, *et al.* Mangiferin alleviated poststroke cognitive impairment by modulating lipid metabolism in cerebral ischemia/reperfusion rats. *Eur J Pharmacol* 2024, 977: 176724.
29. Wang R, Pu H, Ye Q, Jiang M, Chen J, Zhao J, *et al.* Transforming growth factor beta-activated kinase 1-dependent microglial and macrophage responses aggravate long-term outcomes after ischemic stroke. *Stroke* 2020, 51: 975–985.
30. Zhang XS, Lu Y, Li W, Tao T, Wang WH, Gao S, *et al.* Cerebroprotection by dioscin after experimental subarachnoid haemorrhage *via* inhibiting NLRP3 inflammasome through SIRT1-dependent pathway. *Br J Pharmacol* 2021, 178: 3648–3666.
31. Zhou K, Enkhjargal B, Xie Z, Sun C, Wu L, Malaguit J, *et al.* Dihydrolipoic acid inhibits lysosomal rupture and NLRP3 through lysosome-associated membrane protein-1/calcium/calmodulin-dependent protein kinase II/TAK1 pathways after subarachnoid hemorrhage in rat. *Stroke* 2018, 49: 175–183.
32. Lan X, Han X, Li Q, Yang QW, Wang J. Modulators of microglial activation and polarization after intracerebral haemorrhage. *Nat Rev Neurol* 2017, 13: 420–433.
33. Zhang Z, Zhang Z, Lu H, Yang Q, Wu H, Wang J. Microglial polarization and inflammatory mediators after intracerebral hemorrhage. *Mol Neurobiol* 2017, 54: 1874–1886.
34. Tao T, Liu GJ, Shi X, Zhou Y, Lu Y, Gao YY, *et al.* DHEA attenuates microglial activation *via* induction of JMJD3 in experimental subarachnoid haemorrhage. *J Neuroinflammation* 2019, 16: 243.
35. Köchl R, Thelen F, Vanes L, Brazão TF, Fountain K, Xie J, *et al.* WNK1 kinase balances T cell adhesion versus migration *in vivo*. *Nat Immunol* 2016, 17: 1075–1083.
36. Perry JSA, Morioka S, Medina CB, Iker Etchegaray J, Barron B, Raymond MH, *et al.* Interpreting an apoptotic corpse as anti-inflammatory involves a chloride sensing pathway. *Nat Cell Biol* 2019, 21: 1532–1543.
37. Arai Y, Asano K, Mandai S, Ando F, Susa K, Mori T, *et al.* WNK1-TAK1 signaling suppresses lipopolysaccharide-induced cytokine production and classical activation in macrophages. *Biochem Biophys Res Commun* 2020, 533: 1290–1297.
38. Shekarabi M, Zhang J, Khanna AR, Ellison DH, Delpire E, Kahle KT. WNK kinase signaling in ion homeostasis and human disease. *Cell Metab* 2017, 25: 285–299.
39. Bhuiyan MIH, Young CB, Jahan I, Hasan MN, Fischer S, Meor Azlan NF, *et al.* NF- κ B signaling-mediated activation of WNK-SPAK-NKCC1 cascade in worsened stroke outcomes of ang II-hypertensive mice. *Stroke* 2022, 53: 1720–1734.
40. Brown A, Meor Azlan NF, Wu Z, Zhang J. WNK-SPAK/OSR1-NCC kinase signaling pathway as a novel target for the treatment of salt-sensitive hypertension. *Acta Pharmacol Sin* 2021, 42: 508–517.
41. Panda C, Voelz C, Habib P, Mevissen C, Pufe T, Beyer C, *et al.* Aggregated tau-PHF6 (VQIVYK) potentiates NLRP3 inflammasome expression and autophagy in human microglial cells. *Cells* 2021, 10: 1652.
42. Dodd WS, Noda I, Martinez M, Hosaka K, Hoh BL. NLRP3 inhibition attenuates early brain injury and delayed cerebral vasospasm after subarachnoid hemorrhage. *J Neuroinflammation* 2021, 18: 163.
43. Liu FY, Cai J, Wang C, Ruan W, Guan GP, Pan HZ, *et al.* Fluoxetine attenuates neuroinflammation in early brain injury after subarachnoid hemorrhage: A possible role for the regulation of TLR4/MyD88/NF- κ B signaling pathway. *J Neuroinflammation* 2018, 15: 347.
44. Jiang G, Cai Y, Cheng D, Wang H, Deng G, Xiang D. CYLD alleviates NLRP3 inflammasome-mediated pyroptosis in osteoporosis by deubiquitinating WNK1. *J Orthop Surg Res* 2024, 19: 212.
45. Bird L. Innate immunity: Linking mitochondria and microbes to inflammasomes. *Nat Rev Immunol* 2012, 12: 229.
46. Chen S, Ma Q, Krafft PR, Hu Q, Rolland W 2nd, Sherchan P, *et al.* P2X7R/cryopyrin inflammasome axis inhibition reduces neuroinflammation after SAH. *Neurobiol Dis* 2013, 58: 296–307.
47. Dbouk HA, Weil LM, Sachith Perera GK, Dellinger MT, Pearson G, Brekken RA, *et al.* Actions of the protein kinase WNK1 on endothelial cells are differentially mediated by its substrate kinases OSR1 and SPAK. *Proc Natl Acad Sci U S A* 2014, 111: 15999–16004.
48. de Los Heros P, Alessi DR, Gourlay R, Campbell DG, Deak M, MacArtney TJ, *et al.* The WNK-regulated SPAK/OSR1 kinases directly phosphorylate and inhibit the K⁺-Cl⁻ co-transporters. *Biochem J* 2014, 458: 559–573.
49. McCormick JA, Ellison DH. The WNKs: Atypical protein kinases with pleiotropic actions. *Physiol Rev* 2011, 91: 177–219.

Springer Nature or its licensor (e.g. a society or other partner) holds exclusive rights to this article under a publishing agreement with the author(s) or other rightsholder(s); author self-archiving of the accepted manuscript version of this article is solely governed by the terms of such publishing agreement and applicable law.